

A conventional fixation volume electron microscopy protocol for plants

Janithri S. Wickramanayake^{a,b} and Kirk J. Czymmek^{a,b,*}

^aDonald Danforth Plant Science Center, Saint Louis, MO, United States

^bAdvanced Bioimaging Laboratory, Donald Danforth Plant Science Center, Saint Louis, MO,
United States

*Corresponding author: e-mail address: kczymmek@danforthcenter.org

Chapter outline

1	Introduction	84
2	Rationale	85
3	Methods	86
3.1	(Day 1) Primary fixation.....	86
3.2	(Day 2) Secondary fixation and initiation of heavy metal staining.....	89
3.2.1	OTO/Potassium ferrocyanide steps.....	89
3.2.2	Uranyl acetate and lead aspartate staining.....	89
3.3	(Day 3) Heavy metal staining continued and dehydration.....	89
3.4	(Day 4) Dehydration continued and resin infiltration.....	90
3.5	(Day 5) Resin infiltration continued.....	91
3.6	(Day 6) Resin infiltration continued.....	91
3.7	(Day 7) Resin infiltration continued.....	91
3.8	(Day 8) Resin infiltration and polymerization.....	91
3.9	Mounting and SBF-SEM imaging.....	91
3.10	Segmentation and visualization.....	92
4	Instrumentation and materials	92
5	Discussion	94
	Acknowledgments	96
	References	96

Abstract

Volume electron microscopy techniques play an important role in plant research from understanding organelles and unicellular forms to developmental studies, environmental effects and microbial interactions with large plant structures, to name a few. Due to large air voids central vacuole, cell wall and waxy cuticle, many plant tissues pose challenges when trying to achieve high quality morphology, metal staining and adequate conductivity for high-resolution volume EM studies. Here, we applied a robust conventional chemical fixation strategy to address the special challenges of plant samples and suitable for, but not limited to, serial block-face and focused ion beam scanning electron microscopy. The chemistry of this protocol was modified from an approach developed for improved and uniform staining of large brain volumes. Briefly, primary fixation was in paraformaldehyde and glutaraldehyde with malachite green followed by secondary fixation with osmium tetroxide, potassium ferrocyanide, thiocarbonylhydrazide, osmium tetroxide and finally uranyl acetate and lead aspartate staining. Samples were then dehydrated in acetone with a propylene oxide transition and embedded in a hard formulation Quetol 651 resin. The samples were trimmed and mounted with silver epoxy, metal coated and imaged via serial block-face scanning electron microscopy and focal charge compensation for charge suppression. High-contrast plant tobacco and duckweed leaf cellular structures were readily visible including mitochondria, Golgi, endoplasmic reticulum and nuclear envelope membranes, as well as prominent chloroplast thylakoid membranes and individual lamella in grana stacks. This sample preparation protocol serves as a reliable starting point for routine plant volume electron microscopy.

1 Introduction

Plant biology has benefited tremendously from electron microscopy over the decades. More traditional forms using ambient conventional fixation and transmission electron microscopy (TEM), including electron tomography (ET), are routinely used to reveal the common and unique features of plants including the Golgi apparatus (Otegui & Pennington, 2019), plasmodesmata (Sankoh & Burch-Smith, 2021), chloroplasts (Bussi et al., 2019) and plant–microbe interactions (Ivanov et al., 2019). Due to their size, most multicellular plant organisms require high-pressure freezing (HPF) and freeze-substitution to realize the full benefits of cryogenic preservation for TEM (Bourett, Czymmek, & Howard, 1999; Gilkey & Staehelin, 1986). More recently, cryopreservation in combination with direct visualization of unstained, vitrified and frozen-hydrated specimens via scanning electron microscopy (cryo-SEM) (Sviben et al., 2016) and cryoET (Engel et al., 2015; Guo et al., 2022; Weiner et al., 2022) is showing great promise, although thus far largely in unicellular algae such as *Chlamydomonas* sp. While TEM of ultra- and semi-thin sections has been repeatedly demonstrated as an invaluable approach for many plant studies, three-dimensional (3D) visualization, quantification and multiscale perspectives are relatively limited in these highly dimensional and compartmentalized organisms. Indeed, volume electron microscopy (vEM) is well positioned to fill the knowledge gap from the nanoscale to tissue level both independently or in combination with X-ray microscopy and 3D optical approaches. A breadth of biological questions have

been addressed in plant specimens using focused ion beam scanning electron microscopy (FIB-SEM) and serial block-face scanning electron microscopy (SBF-SEM). For instance, FIB-SEM has been employed to study chloroplast-related morphology including quantification of starch (Crumpton-Taylor et al., 2012), chloroplast shape and count, environmental effects or mutant studies (Flori et al., 2018; García-Cerdán et al., 2020; Oi et al., 2017, 2020; Pipitone et al., 2021), for plasmodesmata quantification and distribution in root and viral infected leaf tissues (Paterlini & Belevich, 2022; Reagan & Burch-Smith, 2022) or as general test samples for vEM protocol development (Guo et al., 2020; Roels et al., 2020). SBF-SEM has been leveraged in plants for multiscale correlative imaging with X-ray microscopy (using the same protocol described in detail here) (Duncan et al., 2022), root mutant analysis (Fendrych et al., 2014), quantification of chloroplasts (Bürgy et al., 2021; Harwood et al., 2020), plant cell membranes (Kittelmann, 2018; Kittelmann, Hawes, & Hughes, 2016) and anther development. All of the abovementioned vEM studies invariably used osmium-thiocarbohydrazide-osmium (OTO) and *en bloc* uranium and/or lead staining to impart required contrast and conductive tissues. Cryo-preservation with freeze-substitution and organic solvent strategy was also successfully applied for SBF-SEM of anther and pollen in *Arabidopsis thaliana* using an exclusively organic solvent-based protocol (Czymmek et al., 2020). Alternatively, a solvent- and aqueous-based freeze-substitution fluid followed by rehydration, fixation and staining lead to further enhanced metallization for freeze-substitution of barley roots and anthers, yeast and nematode specimens (Bélanger et al., 2022). While a number of the aforementioned vEM plant studies leveraged the power and convenience of serial imaging of the rigid resin block-face and were sufficient to answer many biological questions, close inspection revealed that not all vEM fixation and staining protocols were created equal for the inherent challenges with plant EM preparation. In many cases, imaging parameters such as beam dosage, variable pressure, voxel size and resulting signal-to-noise prevented some important features from being clearly discerned. This is despite the features being well within the resolution limits of back-scattered electron detection of a modern field emission SEM and demonstrated in other non-plant systems (Deerinck et al., 2018; Narayan et al., 2014; Tsang et al., 2018). Here, we describe a robust protocol for conventional chemical fixation and improved heavy metal staining of plant leaf samples and suitable for high-resolution SBF-SEM, FIB-SEM and other vEM techniques where consistent and intense plant tissue staining benefits overall sample conductivity, contrast and hence improved lateral and axial resolution.

2 Rationale

In our early vEM efforts in plants, we identified three important refinements that influenced a successful and consistent result, especially in more problematic leaf tissue. First, we sometimes experienced inconsistent metallization throughout the tissue adjacent to, and sometimes within, individual cells. To address this, we applied a modified OTO and heavy metal staining protocol by Hua (Hua, Laserstein, & Helmstaedter, 2015) that was developed for uniform and high-contrast vEM in bulk

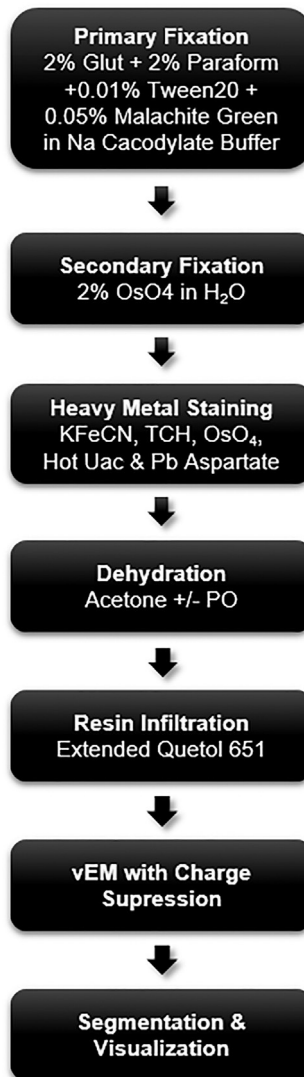
brain tissue. This protocol notably applied potassium ferrocyanide without rinsing following the initial osmium tetroxide fixation in its OTO sequence, and an overnight cold (4 °C) and 2 h hot (50 °C) uranyl acetate as key steps in uniform, high-contrast staining. Furthermore, we ensured that the often buoyant plant leaf tissues were completely submerged in all aqueous fixation and staining steps. Additionally, to enhance contrast in plant cell membranes, we applied the use of malachite green to the primary fixation step. Malachite green has been shown to be effective in stabilizing lipids and enhancing membrane contrast in EM and FIB-SEM of plants, animal tissues and cells in culture (Goetz et al., 2015; Lawton, 1986; Liu et al., 2020). Lastly, to facilitate uniform embedment with the presence of chemically resistant cell walls, cuticle and numerous extracellular air spaces, we applied an extended resin transition with a hard formulation recipe of the low viscosity resin, Quetol 651. The epoxy resin, Quetol 651, is known to significantly improve infiltration with difficult and walled samples (Abad, Cease, & Blanchette, 1988; Ellis, 2016; Martinez & Wick, 1991; Takagi & Sato, 1979). Together, these modifications, in our hands, greatly improved the yield and provided more consistent high-contrast staining with improved conductivity for high-resolution vEM for SBF-SEM and FIB-SEM of difficult plant specimen.

3 Methods

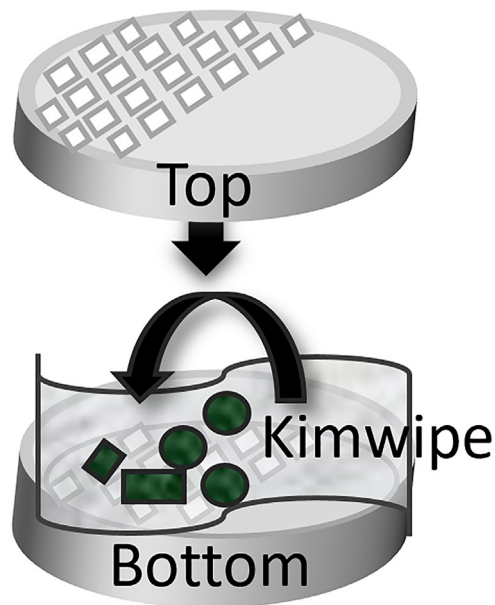
Below, we provide a step-wise walk-through of our modified OTO protocol for plant tissues, based on Hua (Hua et al., 2015). For your convenience, the fixation through to resin steps (Fig. 1) were broken into activities typically performed on each day of processing.

3.1 (Day 1) Primary fixation

- (1) In a chemical fume hood, prepare the fresh primary fixative immediately before excising plant material by creating a final solution with 2% paraformaldehyde, 2% glutaraldehyde, 0.01% Tween-20, 0.05% malachite green in 0.1 M sodium cacodylate buffer (pH 7.4)
- (2) For tobacco leaves, cut small pieces (~5 mm × 5 mm) (avoiding the mid-vein with a double-edged razor blade) or use a 3–5 mm diameter biopsy punch. For safety and to minimize dulling of the cutting-edge, excise or cut the tissue with a large rubber stopper laced on the opposite side of the leaf. Individual duckweed (*Wolffia microscopica*) fronds are <1 mm in any dimension and are processed intact, without cutting
- (3) Immediately place the leaf pieces or fronds into tissue processing cassettes lined with a layer of lens tissue or Kimwipes™ (Fig. 2), folding the Kimwipe to entrap the specimen and prevent the small pieces from escaping the cassette during processing. Then place the cassettes in a specimen container filled with the primary fixative solution at room temperature. The cassettes will keep the

**FIG. 1**

Conventional Fixation vEM Workflow Overview for Plants. This conventional fixation protocol outlines the major steps and chemistries used for successful volume electron microscopy (vEM) in plant tissues. Glut, glutaraldehyde; Paraform, paraformaldehyde; Na, sodium; OsO₄, osmium tetroxide; KFeCN, potassium ferrocyanide; TCH, thiocarbohyrdazide; Uac, uranyl acetate; Pb, lead; PO, propylene oxide.

**FIG. 2**

Cassette for Processing Plant Tissues. Schematic depicting excised circular and rectangular leaf pieces placed on a Kimwipes (and/or lens tissue or equivalent) which is folded over (curved arrow), the top and bottom of the cassette snapped closed and then immediately submerged in primary fixative. The Kimwipes served to prevent small leaf pieces from escaping through cassette openings during processing but can be omitted if the plant tissues exceed cassette opening size.

buoyant leaf samples (due to the hydrophobic waxy cuticle, intercellular air spaces and trichomes) completely submerged during the primary fixation and rinsing steps. Alternatively, small plant leaf and frond samples can be submerged and processed in mPrep/s™ capsules (Microscopy Innovations, Madison, WI, United States) as described previously (Bélanger et al., 2022). Please work quickly from the moment of excision until submersion into fixation to avoid sample desiccation or other related sample manipulation artifacts. This should take no more than 30s/sample

- (4) To aid fixative infiltration into leaf tissue, in a chemical fume hood, place the specimen container without its lid and containing the submerged cassettes with plant tissues into a vacuum desiccator that is connected to house-vacuum. Run at least two 15-min vacuum cycles and then replace the lid securely and gently agitate the samples on a benchtop rotator for 2h (70rpm)
- (5) Replace the primary fixative with a fresh solution containing 2% paraformaldehyde and 2% glutaraldehyde in 0.1 M sodium cacodylate buffer and place the samples at 4 °C overnight

3.2 (Day 2) Secondary fixation and initiation of heavy metal staining

- (6) Moving the samples to a chemical fume hood, open the cassettes and carefully transfer leaf pieces/fronds using tweezers into individual 4 mL glass vials with screw tops containing 0.1 M sodium cacodylate buffer
- (7) Rinse the samples in (5) 10-min changes of 0.1 M sodium cacodylate buffer or until malachite green stain no longer colors the buffer. Place vials with samples onto the benchtop rotator for these rinse steps.

3.2.1 *OTO/Potassium ferrocyanide steps*

- (8) Add 2 mL of 1:1 2% osmium tetroxide (OsO_4):0.2 M sodium cacodylate buffer (in the chemical fume hood) and incubate vials with samples for 4 h at room temperature on the benchtop rotator
- (9) Do not rinse the samples. Pipette off the OsO_4 directly into a hazardous waste container using a plastic transfer pipette and immediately add 2 mL of 2.5% potassium ferrocyanide (specifically, potassium hexacyanoferrate(II) trihydrate) in 0.1 M sodium cacodylate buffer and incubate for 1 h at room temperature on the benchtop rotator
- (10) Rinse the samples twice for 30 min with distilled water (on rotator)
- (11) Add 2 mL freshly made 1% thiocarbohydrazide (TCH) in H_2O (in the chemical fume hood) and incubate at 45 °C for 1 h.
Note: Pre-heat water to 45 °C before adding TCH. Maintain the temperature at 45 °C and vortex intermittently to get TCH fully into solution. This process may take up to 1 h
- (12) Rinse the samples with warm water at 45 °C for 30 min
- (13) Rinse the samples again with water at room temperature for 15 min
- (14) Add 2 mL of 2% OsO_4 in H_2O (in chemical fume hood) and incubate at room temperature for 1.5 h on benchtop rotator
- (15) Remove OsO_4 directly into a hazardous waste container. Rinse the samples three times with distilled water over 30 min

3.2.2 *Uranyl acetate and lead aspartate staining*

- (16) Add 1 mL of 1% aqueous uranyl acetate to each vial and place it at 4 °C in the dark overnight

3.3 (Day 3) Heavy metal staining continued and dehydration

- (17) Incubate the vials with sample containing 1% uranyl acetate at 50 °C for 2 h
- (18) Let the vials cool to room temperature and pipette off the uranyl acetate into a radioactive waste container using a plastic transfer pipette. Make sure to discard the transfer pipettes in a solid radioactive waste container or as provided by your local regulations
- (19) Rinse the samples three times by adding 4 mL distilled water for 30 min and place on benchtop rotator during this step
- (20) To make Walton's lead aspartate solution, mix 0.04 g L-aspartic acid in 10 mL of distilled water and heat to 60 °C in a 15 mL polypropylene centrifuge tube.

Vortex the tube to ensure the L-aspartic acid is fully in solution. Then add 0.066 g Lead nitrate while maintaining the solution at 60 °C. Adjust the pH to 5.5 with 1 M NaOH (~350 µL). Maintain the temperature at 60 °C (Hua et al., 2015)

- (21) Add 2 mL of lead aspartate to the vials and incubate at 50 °C for 2 h
- (22) Allow the vials to cool to room temperature and rinse in three, 10 min changes of distilled water
- (23) Prepare cold solutions (4 °C) of 25%, 50%, 75%, 95%, 100% and 100% of glass-distilled acetone in water to dehydrate the samples in a graded solvent series. Perform 30-min solution exchanges starting with the lowest concentration. Make sure to fill the vials and place the vials on a benchtop rotator. The protocol can be paused at 75% acetone and left overnight on the benchtop rotator. Leaf and fronds at this step will sink to the bottom of the vial, if they have not already done so, by 75% acetone. All solvent exchange steps must be performed in the chemical fume hood

3.4 (Day 4) Dehydration continued and resin infiltration

- (24) Make a 95% and then two 100% acetone exchanges. It is critical to use dry acetone at the 100% step and always leave a little bit of solvent in the vial to prevent tissues from drying out
- (25) Next, perform (2), 30-min exchanges with 100% propylene oxide (PO). PO is a highly volatile and carcinogenic solvent and while this exchange step can be omitted, it provides more consistent resin infiltration for our heavy metallized plant tissues. Due to low surface tension, use glass pasteur pipettes when adding and removing PO. Make sure to work in a chemical fume hood with proper personal protective equipment (PPE) when handling PO
- (26) Next, samples will be slowly infiltrated with various proportions of PO and hard formulation of Quetol 651/NSA embedding resin. To make the embedding resin, mix 17.5 mL Quetol 651 (Ethylene Glycol Diglycidyl Ether), 27 mL NSA (Nonenyl succinic anhydride) and 5.5 mL NMA (Methyl-5-Norbornene-2,3-Dicarboxylic Anhydride) and mix thoroughly on a magnetic stir plate without heat. For initial resin infiltration exchanges detailed below, do not add the DMP-30 ((2,4,6-Tri(dimethylaminomethyl) phenol) component (an accelerator). Make the resin in the fume hood and wear proper PPE
- (27) Make the following mixtures of PO and resin immediately prior to use in 50 mL polypropylene Falcon tubes and mix well:
 - (a) 3:1 PO/resin, 2:1 PO/resin, 1:1 PO/resin, 1:2 PO/resin and 1:3 PO/resin.
Leftover resin can be stored overnight in 4 °C, and ensure the resin mixture is at room temperature prior to mixing with PO.
- (28) Partially remove the PO from the vials and add 3 mL of the first PO/resin (3:1) mixture. Place the samples on the benchtop rotator (keep the vials upright) for 2–4 h depending on tissue type. Generally, leaf tissues and meristems from monocot plants would be 4 h, while roots and dicot plants, 2 h is adequate. The samples may be left overnight in PO/resin mixtures

3.5 (Day 5) Resin infiltration continued

(29) Continue infiltrating samples with the PO/resin mixtures as described above

3.6 (Day 6) Resin infiltration continued

(30) Infiltrate the samples with freshly prepared 100% resin mixture (Quetol 651 NSA without DMP-30 component) for 4–5 h on a benchtop rotator. Repeat this step one more time, and the vials can be left on the rotator overnight with lids on

3.7 (Day 7) Resin infiltration continued

(31) Mix a fresh 50 mL batch of Quetol 651, NSA and NMA and mix well using a stir plate. Then carefully add 1 mL of DMP-30 and continue mixing for about 30 min. A color change from yellow to deep amber will be observed

(32) Remove the resin mixture without DMP-30 and add 3–4 mL of the resin mixture with DMP-30 and agitate using a benchtop rotator for 4–5 h at room temperature

(33) Repeat this step once and leave overnight to ensure proper infiltration of samples with the fully formulated Quetol 651 resin and DMP-30 accelerator

3.8 (Day 8) Resin infiltration and polymerization

(34) Prepare a fresh resin mixture with DMP-30 as described above

(35) Carefully transfer the contents in each vial into an aluminum dish. If using embedding molds, add a small amount of resin to the bottom of each well and transfer the leaf pieces with a disposable plastic pipette or a wood stick and position as desired. Then slightly overfill the embedding mold wells with resin. Alternatively, the tissues can be transferred to a new aluminum dish with fresh resin mixture

(36) Place the mold/aluminum dishes with plant samples in the oven at 50 °C for 48 h

3.9 Mounting and SBF-SEM imaging

(37) For SBF-SEM, an $\sim 2\text{ mm}^2$ segment of plant tissue is excised, oriented and mounted on a Gatan 3View aluminum pin using 2-part conductive silver epoxy and then placed in an oven at 60 °C until thoroughly dry. Then trim excess resin with a razor blade, and make the blockface itself, flat on an ultramicrotome so that it extends no more than 1 mm from the pin surface/sample interface and sputter coat with gold/palladium. Image plant specimen on a Zeiss GeminiSEM300 equipped with a Gatan 3View at 1.5 kV, 0.8 μs dwell-time, 1 pA probe current with focal charge compensation (Deerinck et al., 2018) or equivalent

On the SBF-SEM, first section the block-face until flat and then acquire a survey image using an appropriate pixel resolution and field-of-view.

In our case, we used a 6000×3000 pixel image size, 122.6 nm pixel size (x-y) at 16-bit depth and then select a region of interest (ROI) for high-resolution subsets (Fig. 3A and B)

- (38) For high-resolution vEM image acquisition, an 8000×8000 pixel ROI (Fig. 3A block box, Fig. 3B) can be used with a 5 nm x-y pixel size, 50 nm z-slice interval and collect adequate serial images to capture the desired cells and tissues to be studied

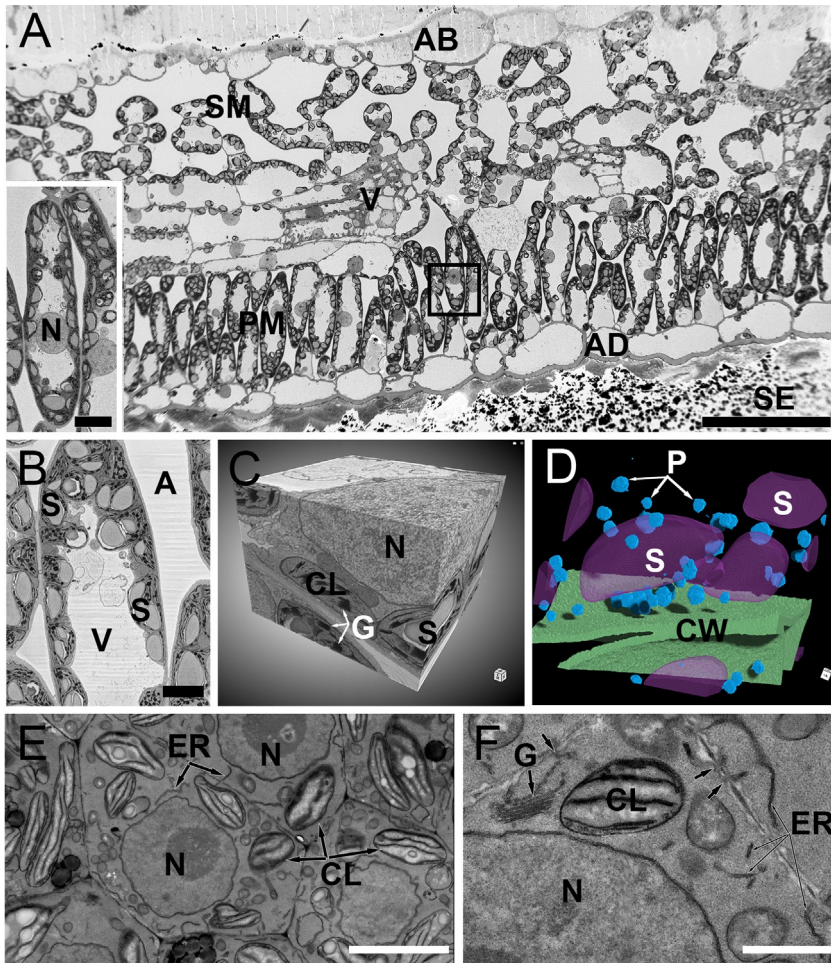
3.10 Segmentation and visualization

- (39) Generate three-dimensional volume renderings using Object Research Systems Dragonfly (Version 2020.2 Build 941). For segmentation and deep learning, a 130 serial image subset of the full stack ROI is processed using the ORS Segmentation Wizard. Fully train three slices (or more if needed) via the manual application of available drawing tools, in this case representing eight cellular features. Apply a four-level Sensor 3D deep learning model with a patch size of 64 to segment various organelles including, but not limited to the plant cell wall, plastoglobules and starch (Fig. 3D)

4 Instrumentation and materials

Instrumentation: Benchtop orbital shaker (SBT300, Southwest Science, Roebing, NJ, United States); Leica Ultracut UCT ultramicrotome (Leica, Buffalo Grove, IL, United States); GeminiSEM 300 with Focal Charge Compensation (Carl Zeiss, Germany); Gatan 3View XP and Gatan Microscopy Suite 3.x (Gatan, Inc., Pleasanton, CA, United States); Dragonfly Pro™ with Deep Learning Module (Object Research Systems, Montréal (Quebec), Canada). TALOS L120C TEM for Life Sciences (TALOSL120C, Thermo Fisher Scientific, Hillsboro, OR, United States).

Materials: Double-edged razor blade (#72000, EMS, Hatfield, PA, United States); biopsy punch (#69031-05, EMS, Hatfield, PA, United States); rubber stopper (14–141 K, Fisher Scientific, Pittsburgh, PA, United States); 38 mm \times 8 mm tissue processing capsules (#62358-W, EMS, Hatfield, PA, United States); mPrep/s Capsules (#22550, Microscopy Innovations, Madison, WI, United States); 4 oz. specimen container (#64231-10, EMS, Hatfield, PA, United States); Nalgene™ vacuum desiccator with Nucelite plate (#5310-0250 and 5312-0230, Thermo Fisher Scientific, Rochester, NY, United States); screw top 4 mL vials (#60992-04, EMS, Hatfield, PA, United States); polypropylene disposable pipettes (#70962-8, EMS, Hatfield, PA, United States); 15 mL polypropylene Falcon tubes (#352196, Fisher Scientific, Pittsburgh, PA, United States); 50 mL polypropylene Fisherbrand™ centrifuge tubes (#06-433-21, Fisher Scientific, Pittsburgh, PA, United States); Corning® glass pasteur pipette and bulbs (CLS7095B9 and Z111597, Sigma-Aldrich, St. Louis, MO, United States); flat embedding molds (#70900, EMS, Hatfield, PA, United States); silver epoxy (Circuit Works, CW2400), Gatan 3-View aluminum pins (Gatan, Inc., Pleasanton, CA, United States); wood applicator sticks (#72300,

**FIG. 3**

A dicot *Nicotiana benthamiana* (tobacco) and monocot *Wolffia microscopica* (duckweed) OTO prepared for vEM. (A) Survey SBF-SEM image of a tobacco leaf cross-section before volume imaging showing the abaxial surface (AB), spongy mesophyll (SM), vascular tissue (V), palisade mesophyll (PM), adaxial surface (AD) and silver epoxy (SE). Black box shows the region of interest (ROI) for high-resolution data in B–D. Scale = 100 μm . (A Inset) Enlarged image of palisade mesophyll cell near block box. N, nucleus. Scale = 10 μm . (B) A representative high-resolution single block-face image from 1A ROI. S, starch; A, apoplast; V, vacuole. Scale = 5 μm . (C) 10 μm^3 rendering of SBF-SEM subset. N, nucleus; CL, chloroplast; G, grana; S, starch. (D) 3D Sensor deep learning segmentation and visualization with ORS Dragonfly™. S, starch; P, plastoglobules; CW, cell wall. (E) The vEM plant protocol applied to duckweed and overview image by TEM showed high-contrast endoplasmic reticulum (ER), chloroplast (CL) and nuclear (N) membrane staining in a frond initial. Scale = 5 μm . (F) High magnification TEM image of duckweed frond initial showed high contrast Golgi (G), chloroplast (CL) membranes, endoplasmic reticulum (ER) and plasmodesmata (arrows). N, nucleus. Scale = 1 μm .

EMS, Hatfield, PA, United States); aluminum trays (#70048, EMS, Hatfield, PA, United States).

Reagents: 16% paraformaldehyde 10mL ampoule (#15710, EMS, Hatfield, PA, United States); 8% glutaraldehyde 10mL ampoule (#16020, EMS, Hatfield, PA, United States); Tween 20 (polyoxyethylene sorbitan monolaurate) (20605, USB Corporation, Cleveland, OH, United States); malachite green oxalate salt (M9015-25G, Sigma-Aldrich, St. Louis, MO, United States); 0.2M sodium cacodylate buffer, pH 7.4 (#11653, EMS, Hatfield, PA, United States); osmium tetroxide 1g ampoule (#19110, EMS, Hatfield, PA, United States); potassium hexacyanoferrate(II) trihydrate, 99% (P9387-100G, Sigma-Aldrich, St. Louis, MO, United States); thiocarbohydrazide (#21900, EMS, Hatfield, PA, United States); uranyl acetate (02624-AB, SPI Supplies, West Chester, PA, United States); L-aspartic acid, reagent grade, $\geq 98\%$ (A9256-100G, Sigma-Aldrich, St. Louis, MO, United States); lead nitrate (#17900, EMS, Hatfield, PA, United States); glass-distilled acetone (#10015, EMS, Hatfield, PA, United States); propylene oxide (#20401, EMS, Hatfield, PA, United States); Quetol 651/NSA kit (#14640, EMS, Hatfield, PA, United States)—kit consists of: Quetol 651 Resin (ethylene glycol diglycidyl ether, #20440), NSA (nonenyl succinic anhydride modified, #19050), NMA (methyl-5-norbornene-2,3-dicarboxylic anhydride, #19000), DMP-30 (#13600).

5 Discussion

Plant biology has long depended on the high-resolution capabilities provided by TEM to visualize cell organelles and other structures (e.g., plasmodesmata, grana, Golgi) that are otherwise limited with photon-based optical approaches. Indeed, numerous examples of vEM applications in plants have been demonstrated with varying degrees of staining intensity, specificity, resolution and biological questions addressed. Furthermore, due to their inherent nature, complex tissues and organs, chemically resistant cell walls and optically scattering properties (apoplastic air spaces and chloroplasts), must be carefully weighed for a quality and successful vEM workflow. The elevated metallization required for SBF-SEM vEM protocols, in particular, are known to result in diffusion fixation and staining quality gradients, especially for large target structures such as brain, kidney or other large multicellular organisms (Mikula et al., 2012; Genoud et al., 2018; Hua et al., 2015). Therefore, we reasoned that some of the species and tissue-dependent fixation and staining inconsistencies that plants are prone to could be alleviated using improved large tissue protocols. While we did not test all of these variations, we did find improvement with a modified Hua protocol, originally used to generate reliable tissue staining in brain (Hua et al., 2015) and also found suitable for correlative X-ray microscopy (XRM) and SBF-SEM (Duncan et al., 2022), the same approach described in more detail herein. It must be noted that one important change we made to the Hua protocol was the addition of malachite green to the primary fixative cocktail. This component has been shown to stabilize and enhance membrane contrast in other systems and likewise, in our study.

As noted, special efforts are required to ensure that buoyant leaf tissue (unlike roots), are adequately submerged in all reagent steps. Despite routine use of the addition of surfactant at low concentration (e.g., Tween 20 or Silwet) and/or gentle vacuum infiltration during primary fixation of some tissues and species, adult or trichrome dense leaves and many monocots (grass and grass-like flowering plants), remain problematic. As such, and similar to our recent efforts with aqueous-based OTO staining following freeze-substitution using carriers such as mPrep/s capsules (Bélanger et al., 2022), or histology-based tissue processing cassettes reported here, all leaf surfaces had adequate contact to the applied chemistries since they were submerged. In general, our OTO treated leaf samples would naturally lose their tendency to float at the air/water interface in the overnight uranyl acetate and/or 75% acetone dehydration steps.

Additionally, we took a “low and slow viscosity” resin approach, selecting a hard Quetol 651 epoxy resin formulation with a viscosity of 15 cP (centipoise) at 25 °C (60 cP formulated) for the added benefit of high contrast morphology due to low resin electron scattering (Kushida, 1974). Quetol’s notable low viscosity compares very favorably to Spurr’s epoxy resin (180 cP with ERL 4221) (Hayden, 2021) or 1:1 Epon 812:Araldite 502 (2500 cP) and various other resin formulations (Ellis, 2016). The Quetol low viscosity was further leveraged by omission of the epoxy accelerator DMP-30 in all graded PO/resin transition steps up to, and including, the first 100% Quetol 651, essentially permitting extended infiltration times (up to 1 day/step) without the inherent and continuous increased viscosity in the presence of DMP-30. The hard formulation of Quetol 651 met our study requirements for 5 nm x-y and 50 nm z-resolution using focal-charge compensation and also suitable for variable pressure in combination with SBF-SEM, however, other well-characterized alternative options for 3D vEM resins (Kizilyaprak et al., 2015; Nguyen et al., 2016) certainly may be considered for substitution with good effect. While plant tissue embedment of our OTO prepared specimen was more reliable using the aforementioned strategy, there is certainly room for further improvement as the occasional residual air apoplastic pockets or infiltration inconsistencies (vascular tissue) were not completely eliminated. The possibility to apply centrifugation (McDonald, 2014) and/or microwave processing (Benhamou et al., 1991; Steyer, Ruhwedel, & Möbius, 2019; Zechmann & Zellnig, 2009) have significant potential to provide additional benefit.

Taken together, we hope the detailed plant tissue protocol described above provides a robust and useful approach for labs that work with plants both infrequently and routinely. We included enhancement for a few critical components that improve the outcome of sample preparation for vEM, especially SBF-SEM and FIBSEM. Namely, substantially improved metallization of the chloroplastic membranes and good staining of the endoplasmic reticulum and plasmodesmata, Golgi, nuclear envelope and plasma membrane (Fig. 3) which made for improved beam stability, speed of acquisition, signal-to-noise and resolution during 3D data collection. Additionally, more reliable and efficient training and segmentation using deep learning (Fig. 3C and D) was possible. Despite these benefits, it must be noted that large air pockets and vacuoles, especially in aerial plant tissues, necessitated some form of charge suppression for consistent SBF-SEM, with focal charge compensation

preferred for highest resolution work with that approach. We also encourage readers to explore the high-pressure freezing and aqueous OTO freeze-substitution variation (Bélanger et al., 2022) of this sample preparation protocol and also consider the merits of correlative X-ray microscopy (Bushong et al., 2015; Duncan et al., 2022; Tsang et al., 2018) to allow contextual and multiscale insights of your target plant specimen. Collectively, the plant research community has many workable vEM approaches at their disposal that can shorten the learning curve and yield a successful outcome for answering many important biological questions not possible with other platforms.

Acknowledgments

We acknowledge the Advanced Bioimaging Laboratory (RRID:SCR_018951) at the Donald Danforth Plant Science Center for optimization of plant sample preparation. We also acknowledge the DOE BER (DBI-0116650) to K. Czymmek and Doug Allen and Kevin Chu (Danforth Center) for providing tobacco plants, Kevin Cox and Blake Meyers (Danforth Center) for providing duckweed. Finally, we thank Lisa Chan, Joel Mancuso and Ruth Redman (Zeiss) for their support with acquisition of SBF-SEM datasets and Rachna Parwani, Robin White with deep learning training support.

References

- Abad, A. R., Cease, K. R., & Blanchette, R. A. (1988). A rapid technique using epoxy resin quetol 651 to prepare woody plant tissues for ultrastructural study. *Canadian Journal of Botany-Revue Canadienne de Botanique*, 66, 677–682.
- Bélanger, S., et al. (2022). A versatile enhanced freeze-substitution protocol for volume electron microscopy. *Frontiers in Cell and Development Biology*, 10. <https://doi.org/10.3389/fcell.2022.933376>.
- Benhamou, N., et al. (1991). Microwave energy fixation of plant tissue: An alternative approach that provides excellent preservation of ultrastructure and antigenicity. *Journal of Electron Microscopy Technique*, 17(1), 81–94. <https://doi.org/10.1002/jemt.1060170109>.
- Bourett, T. M., Czymmek, K. J., & Howard, R. J. (1999). Ultrastructure of chloroplast protuberances in rice leaves preserved by high-pressure freezing. *Planta*, 208(4). <https://doi.org/10.1007/s004250050584>.
- Bürgy, L., et al. (2021). Coalescence and directed anisotropic growth of starch granule initials in subdomains of *Arabidopsis thaliana* chloroplasts. *Nature Communications*, 12(1), 1–10. Springer US. <https://doi.org/10.1038/s41467-021-27151-5>.
- Bushong, E. A., et al. (2015). X-ray microscopy as an approach to increasing accuracy and efficiency of serial block-face imaging for correlated light and electron microscopy of biological specimens. *Microscopy and Microanalysis*, 21(1), 231–238. <https://doi.org/10.1017/S1431927614013579.X-ray>.
- Bussi, Y., et al. (2019). Fundamental helical geometry consolidates the plant photosynthetic membrane. *Proceedings of the National Academy of Sciences of the United States of America*, 116(44), 22366–22375. <https://doi.org/10.1073/pnas.1905994116>.

- Crumpton-Taylor, M., et al. (2012). Control of starch granule numbers in Arabidopsis chloroplasts. *Plant Physiology*, 158(2), 905–916. <https://doi.org/10.1104/pp.111.186957>.
- Czymbek, K., et al. (2020). Imaging plant cells by high-pressure freezing and serial block-face scanning electron microscopy. In M. S. Ortegui (Ed.), *Springer protocols, plant endosomes* (pp. 69–81). Springer US. https://doi.org/10.1007/978-1-0716-0767-1_7.
- Deerinck, T. J., et al. (2018). High-performance serial block-face SEM of nonconductive biological samples enabled by focal gas injection-based charge compensation. *Journal of Microscopy*, 270(2), 142–149. <https://doi.org/10.1111/jmi.12667>.
- Duncan, K. E., et al. (2022). X-ray microscopy enables multiscale high-resolution 3D imaging of plant cells, tissues, and organs. *Plant Physiology*, 188(2), 831–845. <https://doi.org/10.1093/plphys/kiab405>.
- Ellis, E. A. (2016). Quetol 651: Not just a low viscosity resin. *Microscopy Research and Technique*, 79(1), 50–57. <https://doi.org/10.1002/jemt.22597>.
- Engel, B. D., et al. (2015). Native architecture of the Chlamydomonas chloroplast revealed by in situ cryo-electron tomography. *eLife*, 4. <https://doi.org/10.7554/eLife.04889>.
- Fendrych, M., et al. (2014). Programmed cell death controlled by ANAC033/SOMBRERO determines root cap organ size in arabidopsis. *Current Biology*, 24(9), 931–940. <https://doi.org/10.1016/j.cub.2014.03.025>.
- Flori, S., et al. (2018). Imaging plastids in 2D and 3D: Confocal and electron microscopy. *Methods in Molecular Biology*, 1829, 113–122. https://doi.org/10.1007/978-1-4939-8654-5_7.
- García-Cerdán, J. G., et al. (2020). Chloroplast Sec14-like 1 (CPSFL1) is essential for normal chloroplast development and affects carotenoid accumulation in Chlamydomonas. *Proceedings of the National Academy of Sciences of the United States of America*, 117(22), 12452–12463. <https://doi.org/10.1073/pnas.1916948117>.
- Genoud, C., et al. (2018). Fast homogeneous En bloc staining of large tissue samples for volume electron microscopy. *Frontiers in Neuroanatomy*, 12. <https://doi.org/10.3389/fnana.2018.00076>.
- Gilkey, J. C., & Staehelin, L. A. (1986). Advances in ultrarapid freezing for the preservation of cellular ultrastructure. *Journal of Electron Microscopy Technique*, 3(2), 177–210. <https://doi.org/10.1002/jemt.1060030206>.
- Goetz, J. G., et al. (2015). Using correlative light and electron microscopy to study zebrafish vascular morphogenesis. *Tissue Morphogenesis: Methods and Protocols*, 1189, 31–46. https://doi.org/10.1007/978-1-4939-1164-6_3.
- Guo, J., et al. (2020). An optimized approach using cryofixation for high-resolution 3D analysis by FIB-SEM. *Journal of Structural Biology*, 212(1). <https://doi.org/10.1016/j.jsb.2020.107600>.
- Guo, W., et al. (2022). In-situ high-resolution 3D imaging combined with proteomics and metabolomics reveals enlargement of subcellular architecture and enhancement of photosynthesis pathways in nuclear-irradiated Chlorella pyrenoidosa. *Chemical Engineering Journal*, 430(P4), 133037. Elsevier B.V. <https://doi.org/10.1016/j.cej.2021.133037>.
- Harwood, R., et al. (2020). Cell and chloroplast anatomical features are poorly estimated from 2D cross-sections. *New Phytologist*, 225(6), 2567–2578. <https://doi.org/10.1111/nph.16219>.
- Hayden, C. M., & Meseck, E. K. (2021). Transmission electron microscopy of the retina: A method for sample preparation and evaluation. *Toxicologic Pathology*, 49(3), 521–527. <https://doi.org/10.1177/0192623320954124>.

- Hua, Y., Laserstein, P., & Helmstaedter, M. (2015). Large-volume en-bloc staining for electron microscopy-based connectomics. *Nature Communications*, 6, 1–7. Nature Publishing Group. <https://doi.org/10.1038/ncomms8923>.
- Ivanov, S., et al. (2019). Extensive membrane systems at the host–arbuscular mycorrhizal fungus interface. *Nature Plants*, 5(2), 194–203. Springer US. <https://doi.org/10.1038/s41477-019-0364-5>.
- Kittelmann, M. (2018). 3D electron microscopy of the ER. *Methods in Molecular Biology*, 1691, 15–21. https://doi.org/10.1007/978-1-4939-7389-7_2.
- Kittelmann, M., Hawes, C., & Hughes, L. (2016). Serial block face scanning electron microscopy and the reconstruction of plant cell membrane systems. *Journal of Microscopy*, 263(2), 200–211. <https://doi.org/10.1111/jmi.12424>.
- Kizilyaprak, C., et al. (2015). Investigation of resins suitable for the preparation of biological sample for 3-D electron microscopy. *Journal of Structural Biology*, 189(2), 135–146. <https://doi.org/10.1016/j.jsb.2014.10.009>.
- Kushida, H. (1974). A new method for embedding with a low viscosity epoxy resin “Quetol 651”. *Journal of Electron Microscopy*. <https://doi.org/10.1093/oxfordjournals.jmicro.a049928>.
- Lawton, J. R. (1986). The use of malachite green during fixation of plant tissues for the preservation of lipids. *Journal of Microscopy*, 144(2), 201–209. <https://doi.org/10.1111/j.1365-2818.1986.tb02800.x>.
- Liu, Z., et al. (2020). Super-resolution microscopy and FIB-SEM imaging reveal parental centriole-derived, hybrid cilium in mammalian multiciliated cells. *Developmental Cell*, 55(2), 224–236.e6. <https://doi.org/10.1016/j.devcel.2020.09.016>.
- Martinez, L. B., & Wick, S. M. (1991). The use of freeze-substitution and LR gold in the study of rye grass (*Lolium perenne*) pollen. *Journal of Electron Microscopy Technique*, 18(3), 305–314. <https://doi.org/10.1002/jemt.1060180313>.
- McDonald, K. L. (2014). Out with the old and in with the new: Rapid specimen preparation procedures for electron microscopy of sectioned biological material. *Protoplasma*, 251(2), 429–448. <https://doi.org/10.1007/s00709-013-0575-y>.
- Mikula, S., Binding, J., & Denk, W. (2012). Staining and embedding the whole mouse brain for electron microscopy. *Nature Methods*, 9(12), 1198–1201. <https://doi.org/10.1038/nmeth.2213>.
- Narayan, K., et al. (2014). Multi-resolution correlative focused ion beam scanning electron microscopy: Applications to cell biology. *Journal of Structural Biology*, 185(3), 278–284. Elsevier Inc. <https://doi.org/10.1016/j.jsb.2013.11.008>.
- Nguyen, H. B., et al. (2016). Conductive resins improve charging and resolution of acquired images in electron microscopic volume imaging. *Scientific Reports*, 6(November 2015), 1–10. Nature Publishing Group. <https://doi.org/10.1038/srep23721>.
- Oi, T., et al. (2017). Three-dimensional intracellular structure of a whole rice mesophyll cell observed with FIB-SEM. *Annals of Botany*, 120(1), 21–28. <https://doi.org/10.1093/aob/mcx036>.
- Oi, T., et al. (2020). Three-dimensional ultrastructural change of chloroplasts in rice mesophyll cells responding to salt stress. *Annals of Botany*, 125(5), 833–840. <https://doi.org/10.1093/aob/mcz192>.
- Otegui, M. S., & Pennington, J. G. (2019). Electron tomography in plant cell biology. *Microscopy*, 68(1), 69–79. <https://doi.org/10.1093/jmicro/dfy133>.
- Paterlini, A., & Belevich, I. (2022). Serial block electron microscopy to study Plasmodesmata in the vasculature of *Arabidopsis thaliana* Roots. In Y. Benitez-Alfonso, & M. Heinlein, (Eds.), *Plasmodesmata. Methods in Molecular Biology*, 2457. Humana, New York, NY. https://doi.org/10.1007/978-1-0716-2132-5_5.

- Pipitone, R., et al. (2021). A multifaceted analysis reveals two distinct phases of chloroplast biogenesis during de-etiolation in arabidopsis. *eLife*, *10*, 1–32. <https://doi.org/10.7554/eLife.62709>.
- Reagan, B. C., et al. (2022). Focused ion beam-scanning electron microscopy for investigating plasmodesmal densities. In M. Heinlein, & Y. Benitez-Alfonso (Eds.), *Plasmodesmata: Methods and Protocols*. ISBN: 978-1-0716-2131-8, pp. 109–123. https://doi.org/10.1007/978-1-0716-2132-5_6.
- Roels, J., et al. (2020). An interactive ImageJ plugin for semi-automated image denoising in electron microscopy. *Nature Communications*, *11*(1), 1–13. Springer US. <https://doi.org/10.1038/s41467-020-14529-0>.
- Sankoh, A. F., & Burch-Smith, T. M. (2021). Approaches for investigating plasmodesmata and effective communication. *Current Opinion in Plant Biology*, *64*, 102143. <https://doi.org/10.1016/j.pbi.2021.102143>.
- Steyer, A. M., Ruhwedel, T., & Möbius, W. (2019). Biological sample preparation by high-pressure freezing, microwave-assisted contrast enhancement, and minimal resin embedding for volume imaging. *Journal of Visualized Experiments, Im*(145), 1–8. <https://doi.org/10.3791/59156>.
- Sviben, S., et al. (2016). A vacuole-like compartment concentrates a disordered calcium phase in a key coccolithophorid alga. *Nature Communications*, *7*(1), 11228. <https://doi.org/10.1038/ncomms11228>.
- Takagi, I., & Sato, T. (1979). A rapid process for embedding plant tissues in quetol 651 epoxy resin for electron microscopy. *Journal of Electron Microscopy*, *28*(2), 141–144. <https://doi.org/10.1093/oxfordjournals.jmicro.a050162>.
- Tsang, T. K., et al. (2018). High-quality ultrastructural preservation using cryofixation for 3d electron microscopy of genetically labeled tissues. *eLife*, *7*, 1–23. <https://doi.org/10.7554/eLife.35524>.
- Weiner, E., et al. (2022). Electron microscopy for imaging organelles in plants and algae. *Plant Physiology*, *188*(2), 713–725. <https://doi.org/10.1093/plphys/kiab449>.
- Zechmann, B., & Zellnig, G. (2009). Microwave-assisted rapid plant sample preparation for transmission electron microscopy. *Journal of Microscopy*, *233*(2), 258–268. <https://doi.org/10.1111/j.1365-2818.2009.03116.x>.